IOP Conf. Series: Materials Science and Engineering **278** (2017) 012022 doi:10.1088/1757-899X/278/1/012022

Comparison of simulated and experimental results of temperature distribution in a closed two-phase thermosyphon cooling system

E Shaanika[1)], K Yamaguchi[1)], M Miki[1)], T Ida [1)], M Izumi[1)], Y Murase[2)], T Oryu[2)], T Yanamoto[2)]

[1] Tokyo University of Marine Science and Technology, 2-1-6 Etchujima, Koto-ku, Tokyo 135-8533, Japan
[2] Kawasaki Heavy Industries. Ltd, 1-1, Kawasaki-cho, Akashi, Hyogo, 673-8666, Japan

erasmuss03@gmail.com

Abstract. Superconducting generators offer numerous advantages over conventional generators of the same rating. They are lighter, smaller and more efficient. Amongst a host of methods for cooling HTS machinery, thermosyphon-based cooling systems have been employed due to their high heat transfer rate and near-isothermal operating characteristics associated with them. To use them optimally, it is essential to study thermal characteristics of these cryogenic thermosyphons. To this end, a stand-alone neon thermosyphon cooling system with a topology resembling an HTS rotating machine was studied. Heat load tests were conducted on the neon thermosyphon cooling system by applying a series of heat loads to the evaporator at different filling ratios. The temperature at selected points of evaporator, adiabatic tube and condenser as well as total heat leak were measured. A further study involving a computer thermal model was conducted to gain further insight into the estimated temperature distribution of thermosyphon components and heat leak of the cooling system. The model employed boundary conditions from data of heat load tests. This work presents a comparison between estimated (by model) and experimental (measured) temperature distribution in a two-phase cryogenic thermosyphon cooling system. The simulation results of temperature distribution and heat leak compared generally well with experimental data.

1. Introduction

Application of HTS bulk or conductor materials to machinery such as motors and generators could make them lighter, compact and more efficient than conventional machinery. An HTS motor or generator differs from a conventional one in that it would have an HTS field coil or bulks that are cooled by a cryogenic cooling system. In a Thermosyphon-cooled machine, these superconducting coils or bulk materials are installed on the periphery of an evaporator which is located in the rotor cryostat. An adiabatic tube is used to supply the evaporator with liquid cryogen from the condenser located outside the rotor. As such, a cryogenic cooling system is pivotal to superconductor technology applications. Most HTS rotating machines designed thus far have superconducting rotors that operate at 25-68 K[1] . Such cryogenic environments are created and maintained by cryocoolers with the help of Multi-Layer Insulation (MLI) blankets which minimise heat gain [2]. Apart from thermosyphon cooling, other methods for cooling superconductors are forced convection and conduction cooling. In convection cooling, the superconductor is cooled by a forced circulation of a gaseous cryogen. Conduction cooling employs a material with high thermal conductivity to transport thermal energy from the superconductor

to a heat sink. A thermosyphon is a passive heat exchange device that utilizes natural convection to circulate a fluid. It is comprised of three main parts, namely an evaporator, and a condenser connected by an adiabatic tube.

Thermosyphon cooling has been employed in HTS motors and generators where they exhibited advantageous attributes such as high heat flux, near-isothermal operation and simple structure [1-3]. As temperature is a critical factor in superconductor application, it is crucial to study thermal properties of a thermosyphon cooling system such as thermal resistance, heat flux, cooling power and evaporator temperature and heat leak. Some of these thermal properties can only be determined if the temperature distribution of the thermosyphon, especially the evaporator is known. It is therefore useful to have a tool for close estimating temperature distributions. To this end, we studied a scaled down neon thermosyphon. The main objective of this study is to estimate, using simulation, the temperature distribution of the neon thermosyphon cooling system, with aid of experimental data. As such, simulation work was preceded by acquisition of experimental data from the cryogenic thermosyphon cooling system and a subsequent determination of MLI effective emissivity. A thermal model based on temperature was then developed in ANSYS® Workbench based on the experimental data and used to estimate temperature distribution of the thermosyphon components, especially the evaporator, at various filling ratios and heat loads. Simulation results are compared to the experimental data to determine whether the model adequately approximates the real system.

2. Experimental set-up

The thermosyphon cooling system studied in this paper employs neon as working fluid and operates at 30 K. It has a maximum cooling power of 200 W. It is comprised of a cylindrical evaporator which is connected to two condensers with the adiabatic tubes. The horizontal tube is 25.4 mm in diameter and 1200 mm in length. The vertical tube is 34 mm diameter and 800 mm in length as shown in figure 1. The evaporator is made from a 15 mm thick hollow oxygen-free high thermal conductivity copper (OFHC) cylinder sandwiched between two stainless steel flanges. Each condenser is mounted on a cold head of a Cryomech G-M cryocooler. Cold heads were regulated at 29.7 K using Lakeshore temperature controllers. The evaporator, adiabatic tube, condenser as well as the cold heads are wrapped in a MLI and housed in an evacuated cryostat. MLI blankets with 20 layers in total were employed to minimize radiation heat leak from the cryostat. Figure 1 shows the schematic of the thermosyphon system including some physical dimensions.

2.1 *Experimental procedure*

The thermosyphon was filled up with varying neon quantities of 435 NL, 440 NL, 451 NL and 470 NL (NL= Normal Litre: 1 litre at 1 atm and 0 ºC). The neon gas was fed into the system at a pressure of 0.21 MPa and measured with a HORIBA STEC SEC-E40 mass flow controller. Gaseous neon liquefied in the condensers which were regulated at a temperature of 29.7 K and the rejected heat is transferred to the cold heads through the finned heat exchange plates. Liquefied neon flows down the adiabatic tube to the evaporator by gravity. Two polyimide thermofoil heaters attached to the bottom of the evaporator were used to imitate heat generation of a rotor pole. By applying a thermal load using the heaters, neon vaporizes and the gas flows to the condenser, thereby completing the cycle. The temperature of the condensers was monitored thorough LAKESHORE silicon diode temperature sensors attached on the exchange plates. The temperatures at various points of the evaporator and adiabatic tube as well as the thermosyphon internal pressure were measured for each step load. Six of the evaporator temperature sensors are shown in figure 1. Sensor 7 located inside the evaporator measured the temperature near the liquid neon-evaporator interface. The temperature of the cryostat outer surface as well as room temperature was measured and averaged, while total heat leak into the thermosyphon was computed using a Labview function. The evaporator is fitted with viewports through which the liquid neon can be observed. Each thermal load step was maintained for 3 hours to ensure steady-state operating conditions.

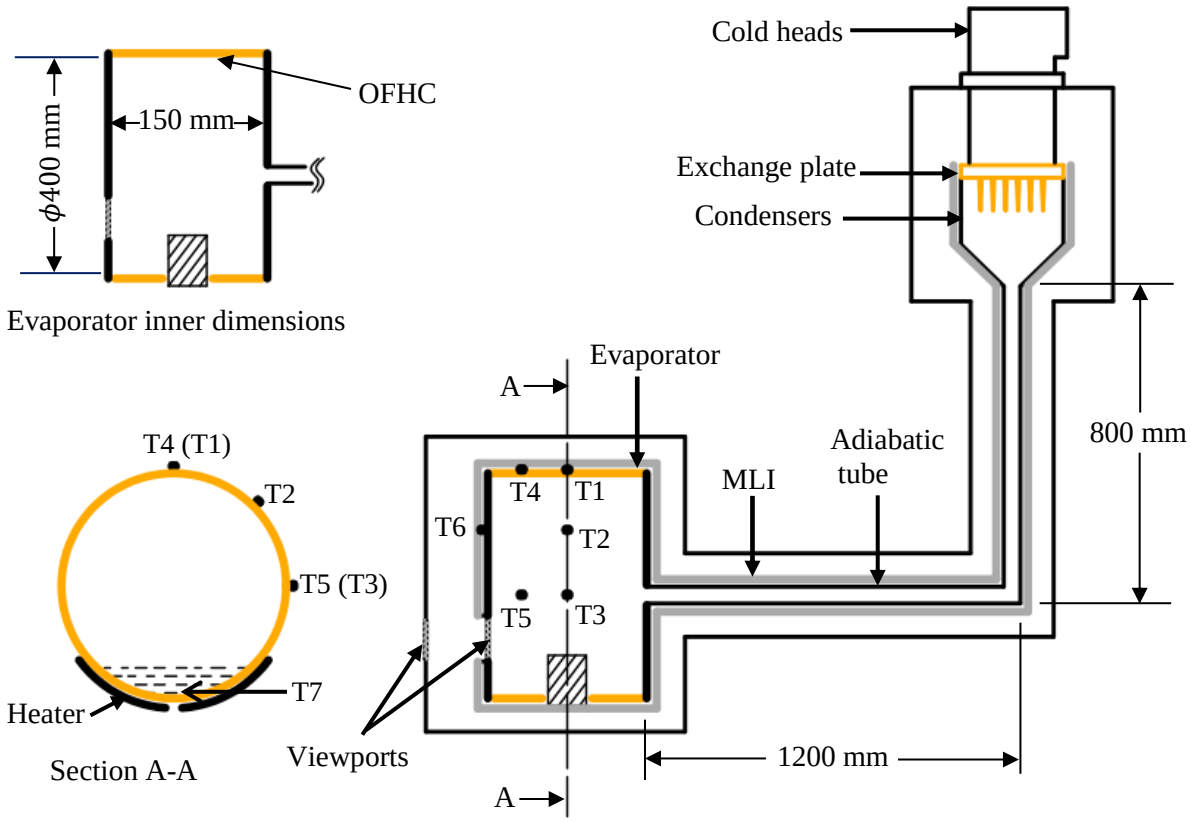

Figure 1. Schematic of the thermosyphon system with the locations of the temperature sensors

3. Heat leak into thermosyphon

Invasive heat comes via convection from ambient air which was at an average temperature of 296.3 K. Heat radiates to the MLI and eventually to the cold mass, while there was heat conduction from the cryostat to the cold mass through structural supports. Heat from instrumentation wires was presumed to be negligibly. Figure 2 is a schematic showing heat transfer mechanisms in the thermosyphon. Knowing the total cooling power (Q_{CH}) of the cold heads at 30 K, cold head temperature regulator heat load (Q_R) and evaporator heat load (Q_E), the total invasive heat could be computed with a Labview program as:

$$\text{Heat leak} = Q_{CH} - Q_R - Q_E \quad (1)$$

3.1. Heat transfer in multi-layer insulation

Two MLI blankets (Ruag Coolcat 2) were utilized to minimize heat gains on the surfaces of the cold mass. Each blanket consisted of 10 layers of low emittance polyester films aluminized on both sides and separated from each other by polyester spacers. Spacers avoid direct contact between adjacent films thus reducing heat conduction between them. Heat transfer through MLI is a combination of radiation, solid conduction and in the presence of a gas, gaseous conduction. Consequently, the efficiency of the MLI is affected by physical composition of the blanket, average blanket temperature as well as mechanical compression. Another factor is the presence of gas or humidity within the layers as MLI is more effective under high order vacuum [4]. We kept the vacuum at about $1x10^{-4}$ Pa, rendering residual gas conduction negligible.

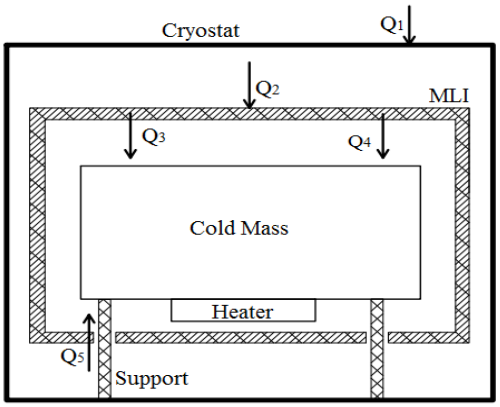

Figure 2. Heat transfer mechanisms in the thermosyphon

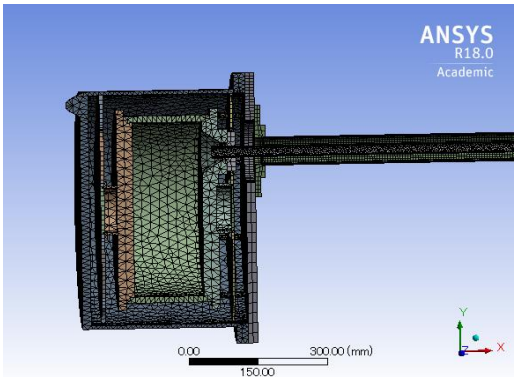

Figure 3. 3D element mesh during simulation of the thermosyphon system

4. Thermosyphon simulation model

A 3D model has been created in ANSYS® Workbench for the thermosyphon cooling system and used to develop a steady-state thermal model. Components that are in contact were modelled with "bonded contact". For each filling ratio, temperature of the adiabatic tube and evaporator, evaporator heat flux, radiation and convection boundary conditions were defined. The program then computed temperature distribution of all objects of the thermosyphon. The subsequent part of this sections describes the thermal model in terms of boundary conditions and assumptions made. Example of 3D element map is shown in figure 3.

4.1. Heat leak in the model

Total heat leak is a sum of heat transfer through the MLI and glass fibre supports of the evaporator. Heat transfer through glass fibre supports to the cold mass is via conduction, while that through the MLI is a combination of radiation and conduction. Gaseous conduction was neglected due to high vacuum level.

4.2. Determination and defining of MLI effective emissivity

Due to the nature of heat transfer in MLI, thermal conductivity of the insulation is not strictly defined in terms of variables such as temperature or physical properties of the component materials. It is therefore plausible to refer either to an apparent thermal conductivity, K_{eff}, or effective emissivity, ε_{eff}. Under high vacuum pressures, the theoretical values of effective conductivity and emissivity can be predicted using equations. However, the actual value for an MLI is usually larger than predicted due to conduction paths created between layers because of penetrations and handling [4].

Thermal conductivity and effective emissivity values can also be derived experimentally from data of a thermal system during steady-state heat transfer [4]. In this study, the thermal effect of the MLI is

modelled with ε_{eff} which is defined as effective emissivity from the cryostat wall, through the MLI to the cold mass. As such, the MLI is modelled as single surface coupled directly to the cold mass it surrounds. This single surface (the MLI) was then assigned an emissivity equal to the effective emissivity. The appropriate effective emissivity value of the MLI was determined using steady-state experimental data of 435 NL. This was done as follows: First a steady-state thermal model such as that in figure 3 was created. The MLI is modelled as a surface surrounding the cold mass in this model. Secondly, a heat load, say 0W, 435 NL is chosen, and its boundary conditions are defined in the thermal model. The effective emissivity value of the MLI surface is then tweaked in an iterative manner until the estimated total heat leak (conduction and radiation) is equal to the measured heat leak value. The value at this point is equal to ε_{eff}. The appropriate effective emissivity value was found as 0.03 and this was the value used to model the thermal effect of MLI in temperature simulations of all heat loads and neon quantities.

The heat transfer equation that models the MLI thermal effect in this case is given by equation 2 [4]:

$$Q = \sigma A_{\text{S}} \varepsilon_{\text{eff}} (T_{\text{S}}^4 - T_{\text{Surr}}^4) \quad [\text{W}] \tag{2}$$

where
Q is the net heat transferred from cryostat through MLI to the cold mass [W];
A_{S} is the surface area of the MLI [m^2];
T_{S} is the temperature of the cold mass which the MLI surrounds [K];
T_{Surr} is the temperature of the enclosing cryostat [K]
σ is the Stefan-Boltzmann Constant [5. 67x10^{-8} W/m^2 K^4].

4.3. Boundary conditions

Convection. Convection heat transfer had been defined between the outer surface of the cryostat and ambient air. Since there was no bulk air movement, a free convection heat transfer coefficient of 5W/m^2 was chosen. The average temperature of ambient air had been computed as 296.3 K.

Radiation. Radiation objects were defined between the cryostat and the MLI. Radiation interaction is obtained by defining an enclosure between objects radiating to each other. The enclosure was further defined as PERFECT, as there was negligible amount of air due to high vacuum. Stainless steel has an emissivity of 0.15, and the effective emissivity (0.03) of the MLI was defined on surfaces directly coupled to the cold mass.

Temperature. The evaporator cryostat is designed with two viewports through which the liquid neon in the evaporator can be observed. So, the neon volume as well as the contact area of liquid neon with the evaporator (the wetted area) could be calculated for each heat load test. The wetted area covered by neon was one of the temperature boundary conditions defined in the thermal model. The temperature of this wetted area is obtained from sensor T7 located at the liquid-evaporator interface. The temperature was defined as such due to temperature continuity- it is assumed that the temperature of the neon at the neon-evaporator interface is the same as that of the evaporator surface. The inside of the adiabatic tube was set to the temperature registered by the liquid neon sensor. Similarly, all other components in contact with liquid neon had temperature boundary conditions defined

Evaporator heat flux. Two model thermofoil heaters were used to apply heat loads to the evaporator. Heat load from of the heaters was applied as heat flux, specified on heater surface and directed onto the evaporator.

5. Results and discussion

Results of heat load tests are shown in figure 4 and figure 5. Figure 4 shows the change of filling ratio with applied heat load. The filling ratio is defined as the ratio of neon liquid volume to total thermosyphon volume. For each neon quantity, the evaporator heat load was systematically increased, causing the filling ratio to decrease until the dry-out limit was reached. Figure 5 shows the increase in temperature that is observed as evaporator heat load is increased until dry out limit for 470 NL. The sensor at the neon-evaporator interface registered the smallest increase of 0.4 K.

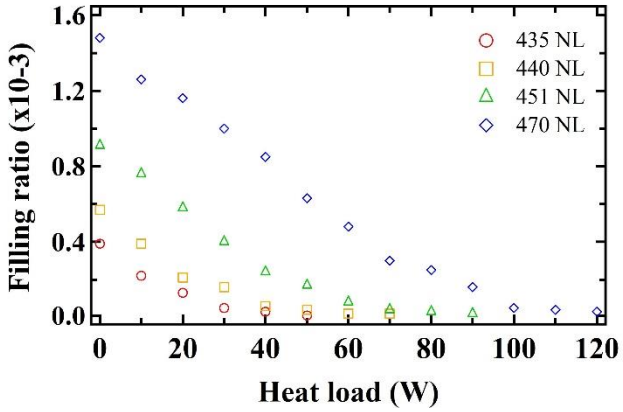

Figure 4. Variation of filling ratio with applied heat load

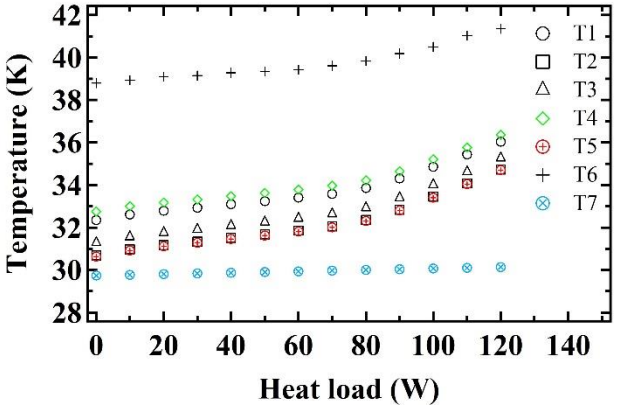

Figure 5. Variation of temperature with applied heat load at 470 NL

5.1. Temperature difference

Difference between estimated and measured (measured – estimated) temperatures are indicated here for the six sensors on the evaporator. Figures 6-9 show the difference between experimental and estimated temperatures for different heat loads. The model estimation under-predicted the temperature at each sensor location compared to the experimental data.

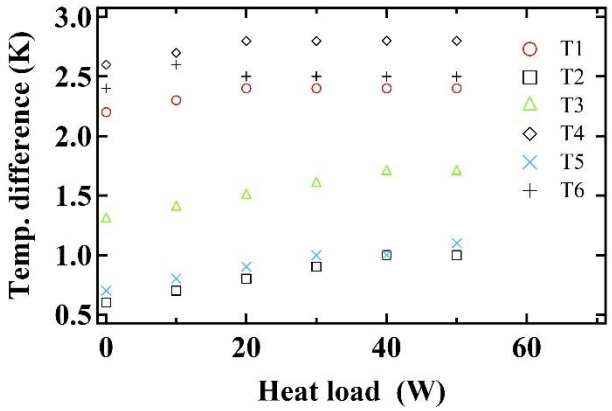

Figure 6. Temperature difference at different heat loads for 435 NL

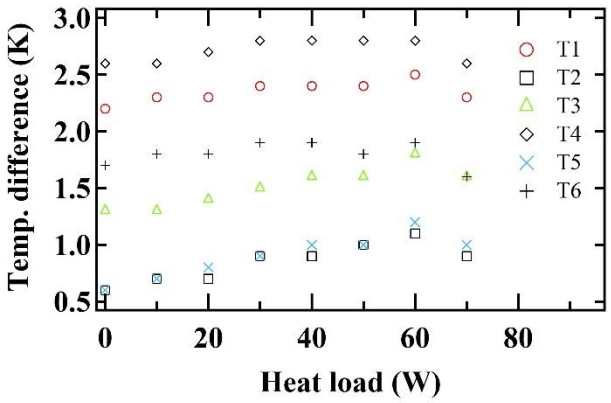

Figure 7. Temperature difference at different heat loads for 440 NL

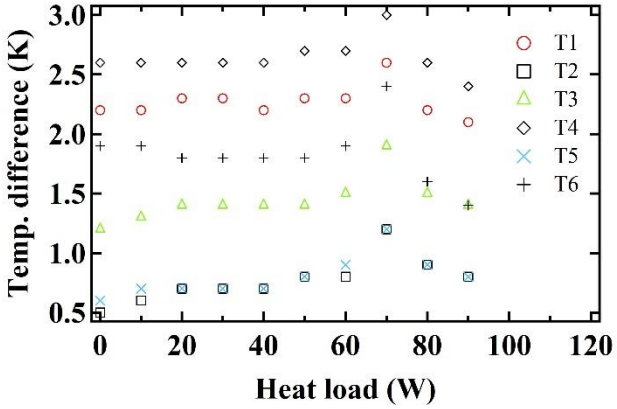

Figure 8. Temperature difference at different heat loads for 451 NL

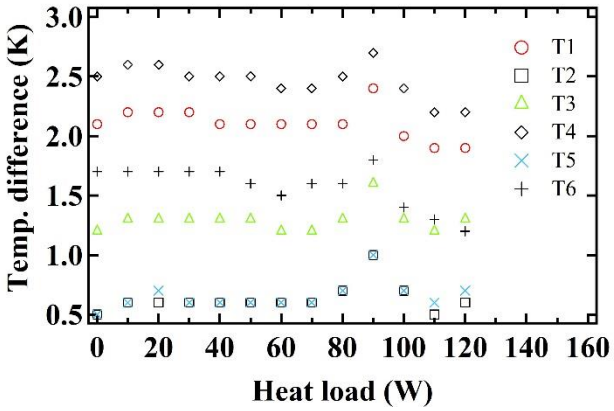

Figure 9. Temperature difference at different heat loads for 470 NL

The sources of difference could be threefold. The first cause could be the simulation 'bonded contact' that was defined between objects in contact. Bonded contacts lead to thermal coupling higher than the actual one. Secondly, the ambient air temperature changes continuously, thus convection may have contributed to the difference. The third cause may be the neon liquid-evaporator contact area, which may account for the concave downward concave shape of the all graphs in figures 6-9. The implication of large difference at these inflection points is that they suggest a change in the boiling regime. Film boiling occurred at high heat loads, leading to a reduced neon-evaporator contact area. During film

boiling, pockets of vapour cover part of the wetted area so that the actual contact area is only a portion of the total wetted area we see through the viewport. This may affect the wetted area temperature boundary condition in that a slightly larger contact area is defined, leading to slightly lower temperature estimates.

5.2. Heat leak

Figure 10 shows the experimental and estimated heat leak. It may be noted here that because the measured heat leak value for 435 NL was used in determining the effective emissivity, the experimental and estimated heat leak values at 435 NL are equal. The estimation is good since the difference is at most 0.8W. Furthermore, the model estimated invasive heat through the MLI to the cold mass accounted to be 48% and conduction heat leak via all the supports to be 52% of the total heat leak.

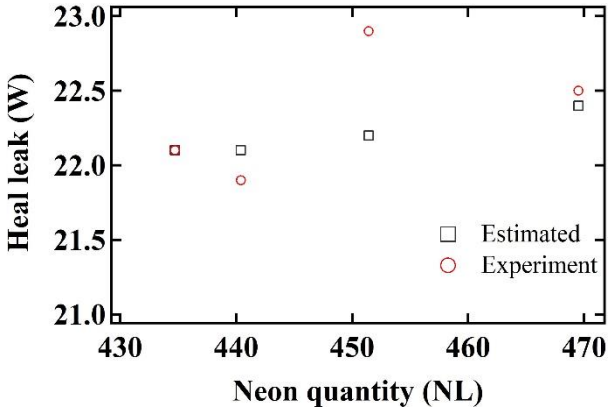

Figure 10. Experimental and estimated heat leak at 0 W of evaporator heater

6. Conclusion

This paper compared experimental distribution and simulated temperature distribution in a closed two-phase thermosyphon. Firstly, experimental results were obtained from neon thermosyphon at various filling ratios and heat loads. Secondly, temperature and heat leak of the thermosyphon were estimated by simulation. The MLI had been modelled using the effective emissivity approach. The proximity of simulation results to experimental data suggests that simulation results may be useful for estimating temperature distribution. The model also provided further insight into how heat leaks into the thermosyphon.

7. References

[1] Yamaguchi K, Motohiro M, Yamagata K, Ikeda T, Kashima H, Izumi M, Murase Y, Yanase E and Yanamoto T 2016 IEEE *Trans. Appl. Supercond.*, vol. **26**, no. 3, 5204405.

[2] Kalsi S, 2011 *Applications of High Temperature Superconductors To Electrical Power Equipment* (New Jersey: John Wiley & Sons Inc) chapter 3 pp 35-58

[3] Gilmore D G, Ed., 2002 *Spacecraft Thermal Control Handbook: Fundamental technologies* vol. **I** (California: The Aerospace Press) chapter 5 pp 161-205

[4] Habte M 2008 Two Phase Closed Thermosyphon Cooling System *Cooling the Moderator of Cold Neutron Source (CNS) for Research Nuclear Reactor* (Pennsylvania: VDM Dr. Mueller Aktiengesellschaft & Co. KG)

[5] Felder B, Miki M, Deng Z, Tsuzuki K, Shinohara N, Izumi M and Hayakawa H 2011 *IEEE Trans. Appl. Supercond*, pp. 2213-16